Available online at www.sciencedirect.com
SCIENCE DIRECT®
Journal of Nuclear Materials 321 (2003) 60–69
journal of nuclear materials
www.elsevier.com/locate/jnucmat

Cyclic stress–strain response of textured Zircaloy-4

Cong Li [a,b,*], Shihao Ying [b], Baoluo Shen [a], Shaoyu Qiu [b], Xuyu Ling [a], Yanfeng Wang [a], Qian Peng [a,b]

[a] School of Materials Science and Engineering, Sichuan University, Chengdu, Sichuan, 610065, People's Republic of China
[b] National Key Laboratory for Nuclear Fuel and Materials, Nuclear Power Institute of China, P.O. Box 436, Chengdu, Sichuan, 610041, People's Republic of China

Received 28 November 2002; accepted 27 March 2003

Abstract

In this paper, the cyclic stress–strain response of textured Zircaloy-4 is investigated at room temperature in an incremental step test using fully reversed tension–compression loading under strain control. The material exhibits an asymmetry of stress response in both rolling and transverse directions, and the corresponding cyclic stress–strain curves can be expressed by a power law relation. Furthermore, phenomenological friction and back stresses are derived from an analysis of hysteresis loop shapes using the Cottrell scheme. It has been shown that the magnitude of the phenomenological friction stress in compression is always higher than that in tension for either rolling or transverse direction. While the magnitude of the phenomenological back stress, being independent of the loading direction, increases much more rapidly in transverse direction than that in rolling direction with increasing the plastic strain amplitude, and the trend in both directions can be expressed by a logarithmic relation. A further discussion suggests that (i) the intergranular thermal stress in the material is responsible for the difference in the phenomenological friction stress between tension and compression, thus leading to the asymmetry of stress response; (ii) the increase of the saturated stress with the plastic strain amplitude stems from the back stress that is primarily a direct consequence of the plastic strain incompatibilities between grains; (iii) the different performance between rolling and transverse directions results from the texture effect.

1. Introduction

Zircaloy-4 is used as the cladding material of nuclear fuel rods in light water reactors, and the rods are subjected to power fluctuations during load following operation. The power fluctuations cause cyclic stresses and strains in the cladding tubes through the process known as pellet-cladding interaction [1]. It is therefore necessary to have an accurate knowledge of the cyclic stress–strain behavior demonstrated by Zircaloy-4 in order to model the fuel rod behavior under normal operating and accident conditions.

The data on the cyclic stress–strain behavior of zirconium and its alloy can be found in [2–6]. The evolution of peak stress response with the number of cycles at different strain amplitude showed that the initial cyclic hardening followed by softening or the only cyclic softening to fracture could be observed for both recrystallized Zircaloy-4 [2] and recrystallized zirconium [3], which seem to contradict the findings [4] that a recrystallized Zircaloy-4 cyclically hardens and the kinetics of hardening depends considerably on the strain range. Nevertheless, the comparison between cyclic stress–strain curve and monotonic stress–strain curve shows that the recrystallized material displays cyclic hardening [3–5], whereas the cold-worked material exhibits cyclic

* Corresponding author. Address: National Key Laboratory for Nuclear Fuel and Materials, Nuclear Power Institute of China, P.O. Box 436, Chengdu, Sichuan 610041, People's Republic of China. Tel.: +86-28 85903379; fax: +86-28 85906023.
E-mail address: licong@npic.ac.cn (C. Li).

0022-3115/$ - see front matter © 2003 Elsevier B.V. All rights reserved.
doi:10.1016/S0022-3115(03)00200-9

hardening at room temperature, cyclic softening at elevated temperature [6].

It is generally accepted that the cyclic flow stress can be divided into two components, phenomenological 'friction stress σ_f' and 'back stress σ_b', from hysteresis loop shapes using Cottrell's scheme [7]. In accordance with the Cottrell's scheme as expressed by Kuhlmann-Wilsdorf and Laird [8] in single crystal, one can have the following depictions as shown in Fig. 1. At the onset of the plastic deformation in the tension-loading direction of a cycle, i.e. at σ_y^t, a back stress σ_b^t has been generated in the preceding cycle. Thus, in the presence of a friction stress σ_f^t one can write

$$\sigma_y^t = \sigma_f^t - \sigma_b^t. \tag{1}$$

However, at the end of the forward cycle, when the back stress has reached its maximum value but now counteracts instead of aids the deformation, the stress is the sum instead of the difference of the friction and back stresses, i.e.

$$\sigma_s^t = \sigma_f^t + \sigma_b^t \tag{2}$$

and therefore,

$$\sigma_f^t = (\sigma_s^t + \sigma_y^t)/2, \tag{3}$$

$$\sigma_b^t = (\sigma_s^t - \sigma_y^t)/2. \tag{4}$$

Similarly, one can have the following relations:

$$\sigma_f^c = (\sigma_s^c + \sigma_y^c)/2, \tag{5}$$

$$\sigma_b^c = (\sigma_s^c - \sigma_y^c)/2, \tag{6}$$

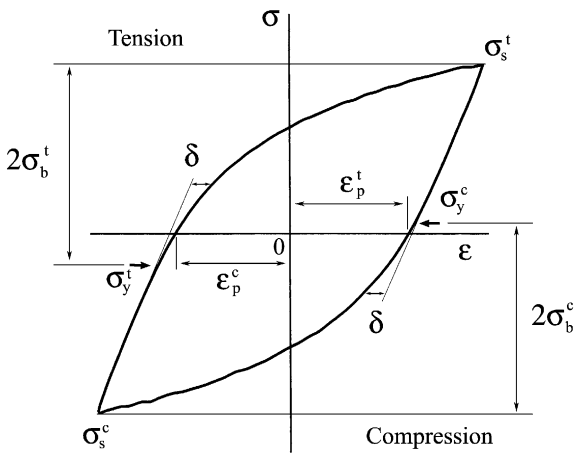

Fig. 1. Definition of yield stress, saturated stress, and phenomenological back stress in the hysteresis loop.

where σ_y^c, σ_f^c and σ_b^c are the yield, friction and back stresses in the compression-loading direction of the cycle, respectively. Note that σ_y^t and σ_y^c are determined on the basis of a deviation from linearity with a coefficient $\delta = 10^{-4}$ as shown in Fig. 1, respectively.

Using the Cottrell scheme to determine the back and friction stresses of zirconium and its alloy, both Choi et al. [9] and Crépin et al. [10] took the hysteresis loops as symmetrical, as treated in single crystal [8] and cubic metals [11]. Nevertheless, they overlooked the asymmetrical deformation behavior of Zircaloy-4 that consists of flow stress in compression which was always higher than that in tension [4,10]. So, a special attention should be given to the asymmetry of hysteresis loops for zirconium and its alloys when applying the Cottrell scheme to estimate the back and friction stresses. On the other hand, the study on friction and back stresses versus the plastic strain amplitude is not yet reported for zirconium and its alloys.

Due to the limited deformation modes, fabrication of the cladding tube will produce a pronounced texture in Zircaloy-4 [12]. Nevertheless, there is still a lack of detailed studies on the effect of texture on cyclic stress–strain behavior of Zircaloy-4.

The purpose of this paper is to give a further insight into the cyclic stress–strain response by an analysis of the accompanying changes in the shapes of the hysteresis loops, and to examine the impact of texture on the cyclic stress–strain response of Zircaloy-4.

2. Material and experimental procedure

2.1. Material

The material investigated in this study is a Zircaloy-4 plate of the composition given in Table 1. The plate was cold-rolled to a sheet with a thickness of 1.2 mm, and then subsequently annealed at 580 °C for 2 h in vacuum, which resulted in an equiaxed grain microstructure of ~8 μm in size.

Textures are characterized by pole figure and Kearn's factor where the sheet-normal, transverse, and rolling directions are denoted as ND, TD, and RD. Kearn's factor is a texture coefficient, defined in terms of the effective fraction of crystals with their basal poles parallel to a particular direction [13]. The sheet has the typical texture for Zircaloy-4 sheet [14]. The Kearn's factors are 0.576, 0.138, 0.288 for ND, RD, and TD,

Table 1
Chemical composition of the material (mass%)

Tin	Iron	Chromium	Oxygen	Zirconium
1.45	0.21	0.11	0.12	Bal.

respectively. It indicates that the basal poles in the sheet are concentrated close to the ND and the pole intensity decreases away from it in each direction. Higher values of Kearn's factor along the TD than those along the RD indicates that more basal poles are aligned in the transverse direction when compared to those in the rolling direction.

The ND, RD, and TD inverse pole figures show that most of the basal poles are oriented close to the ND and prismatic poles are mostly along the RD and the TD. The basal and prismatic pole figures for the sheet are shown in Fig. 2. The center of Fig. 2(a) corresponds to the ND, Fig. 2(b) and (c) to the RD and TD, respectively. The basal pole figure (Fig. 2(a)) clearly reveals the typical bimodal distribution of the basal poles concentrated in the transverse (ND–TD) plane normal to the rolling direction of the sheet, the maximum relative intensity of the basal pole peaks (3.7 times random) appears at $\pm 25°$ from the sheet normal direction towards the transverse direction in the ND–TD plane. The prismatic poles with the maximum relative intensity of 3.1 times random are parallel to the rolling direction (Fig. 2(b)) while some prismatic poles with the maximum relative intensity of 1.8 times random can be found in the transverse direction (Fig. 2(c)). This permits to conclude that the prismatic poles are more concentrated in the rolling direction as compared to those in the transverse direction. As it is assumed for recrystallized Zircaloy [15], the prismatic poles would present a maximal intensity at $\sim 30°$ from the RD towards the TD. However, no such peak (see Fig. 2(b)) appears. It hints that the present sheet is still partially recrystallization state from the texture point of view.

2.2. Cyclic deformation test

The specimens having hourglass profile, as shown in Fig. 3, are of two types. One has the loading direction parallel to the rolling direction (designated as R specimen), and the other has the loading direction parallel to the transverse direction (designated as T specimen). This specimen design is similar to one used by Wisner et al. [16].

The specimen is so thin that buckling would occur easily. In order to avoid buckling during test, a fixture was designed and used to rigidly grip sample and accurately transmit cyclic load along the longitudinal specimen axis.

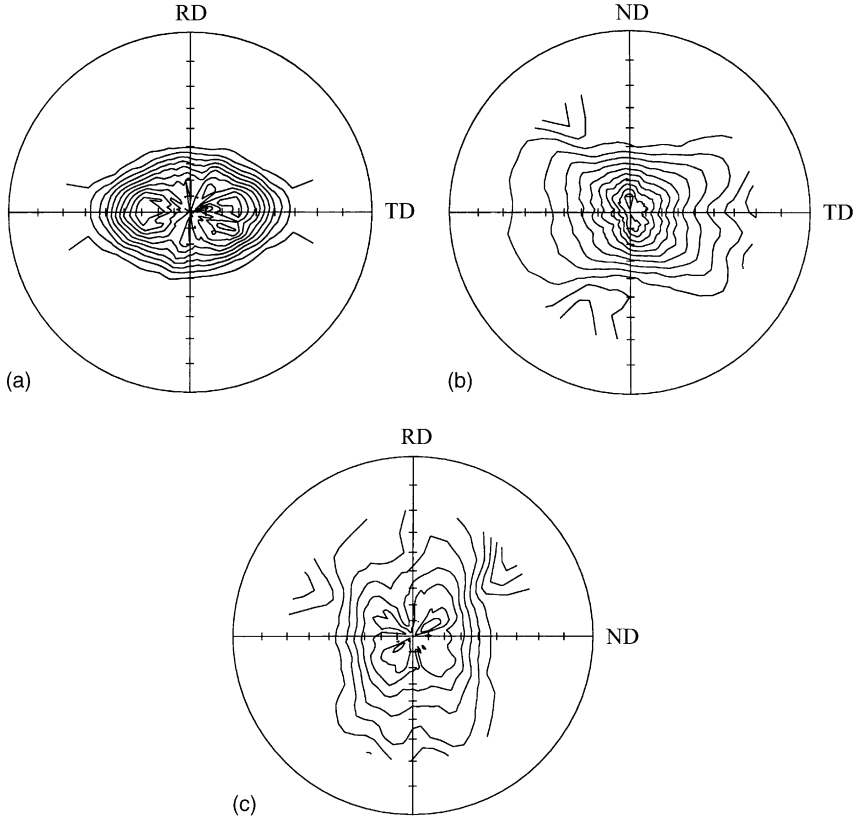

Fig. 2. (a) (0 0 0 2) pole figure, the center corresponds to ND. (b) $(10\bar{1}0)$ pole figure, the center corresponds to RD. (c) $(10\bar{1}0)$ pole figure, the center corresponds to TD.

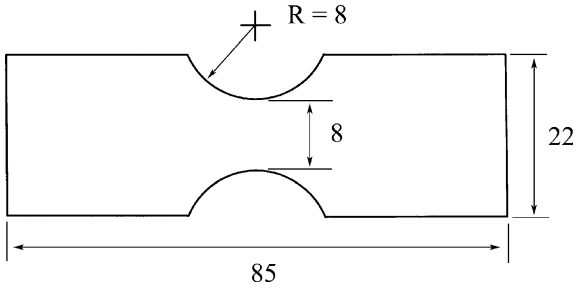

Fig. 3. Specimen geometry.

Before the tests, each specimen was chemically polished using a mixture of H_2O, HNO_3 and HF (H_2O:HNO_3:HF = 45:45:10, vol.). The cyclic stress–strain curves were obtained with an 809 MTS (25 kN) servohydraulic test machine using an incremental step test, whereby the specimen was subjected to a series of blocks of stepwise with increasing the total strain. For each specimen the total strain was increased from 0.1% up to 1.50% by a strain interval, and the specimen was cycled for 50 cycles at each given total strain with a constant nominal strain rate of 2×10^{-3} s^{-1} in symmetrical conditions ($R_\varepsilon = \varepsilon_{min}/\varepsilon_{max} = -1$). The total strain range was controlled across the minimum width of the specimen in accordance with the ASTM standard E606 [17], and therefore the total strain amplitude ε_t and plastic strain amplitude ε_p in the loading direction can be obtained using the method in the ASTM standard E606.

3. Results

3.1. Stress response

For both R and T specimens, the stress range always decreases slightly with the number of cycles, it indicates that the material shows cyclic softening behavior at room temperature, at least initial cyclic softening, which are compatible with the findings of Lee et al. [2,9]. In about 40 cycles for the different strain levels the hysteresis loops are approximately stabilized, as shown in Fig. 4. The shapes of the hysteresis loops depend significantly on the strain amplitude. The hysteresis loops are narrow at very low strain, and the peak stress increases and the loop becomes wide with increasing ε_t.

The cyclic stress–strain curves, as shown in Fig. 5, are obtained by connecting the tips of hysteresis loops at 50th cycle for various strain amplitudes, which could be expressed by a power law relation:

$$\sigma_s = K^s \varepsilon_p^{n^s}, \tag{7}$$

where σ_s (MPa) is the magnitude of the saturated stress for a plastic strain amplitude ε_p, K^s is the cyclic strength coefficient and n^s is the cyclic work hardening exponent. These parameters are given in Table 2 for both samples.

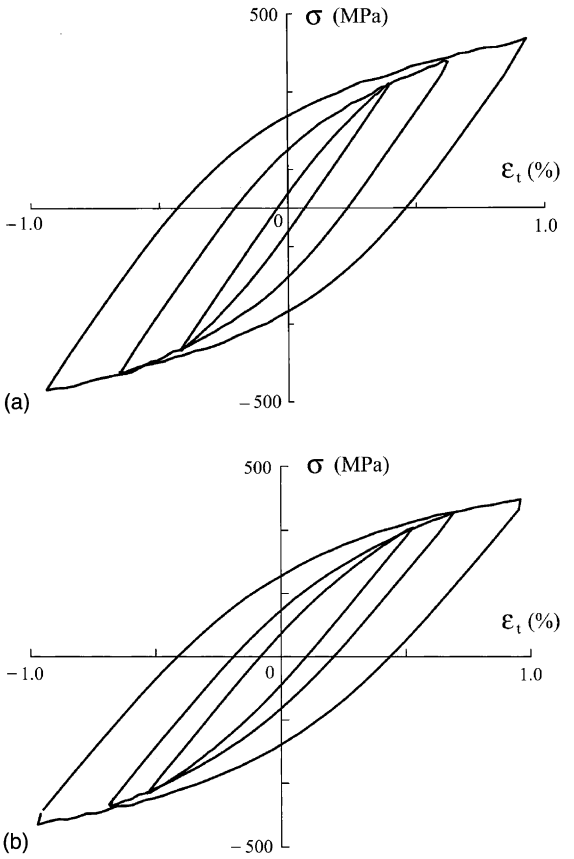

Fig. 4. Shapes of hysteresis loops. (a) Sample R; (b) sample T.

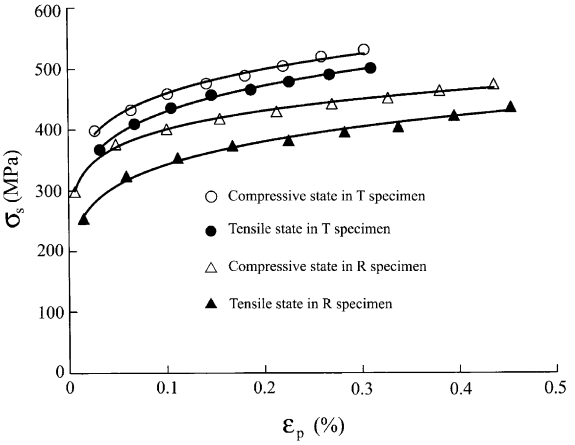

Fig. 5. Cyclic stress–strain curves derived from the hysteresis loops.

As shown in Fig. 5, the magnitude of saturated stress in compression (σ_s^c) is always higher than that in tension (σ_s^t) with a stress ratio of $\sigma_s^t/\sigma_s^c < 1$, and the stress ratio increases slightly with increasing ε_p. In addition,

Table 2
Parameters from the equation $\sigma_s = K^s \varepsilon_p^{n^s}$

Sample	K^s (MPa)	n^s	R^2
R in tension	970.2	0.1507	0.9912
R in compression	831.49	0.1057	0.9965
T in tension	1086.9	0.1342	0.9974
T in compression	1043.1	0.1186	0.9909

saturated stress of T specimen in either tension or compression is always higher than R specimen at the same ε_p. Note that the stress ratio for R specimen is always lower than T specimen at any ε_p, indicating that the asymmetry of stress response for R specimen is more pronounced than T specimen.

3.2. Back and friction stresses

Fig. 6 depicts the variations of the magnitude of back stress σ_b with ε_p. The magnitude of σ_b^t for either R specimen or T specimen appears to be identical to that of σ_b^c. This permits to conclude that the magnitude of σ_b is roughly independent of the loading direction, i.e. $\sigma_b^t = \sigma_b^c$. Moreover, the magnitude of σ_b is always higher in T specimen than R specimen, and the magnitude difference between both samples becomes more remarkable with increasing ε_p. While, the magnitude of σ_b for both samples exhibits a logarithmic increase as a function of ε_p:

$$\sigma_b = K^b \ln \varepsilon_p + C_b, \tag{8}$$

where K^b is the logarithmic coefficient and C_b is the constant, which are given in Table 3.

The variations for the magnitude of friction stress with ε_p are shown in Fig. 7. For both samples, friction stress in magnitude decreases slightly with increasing ε_p

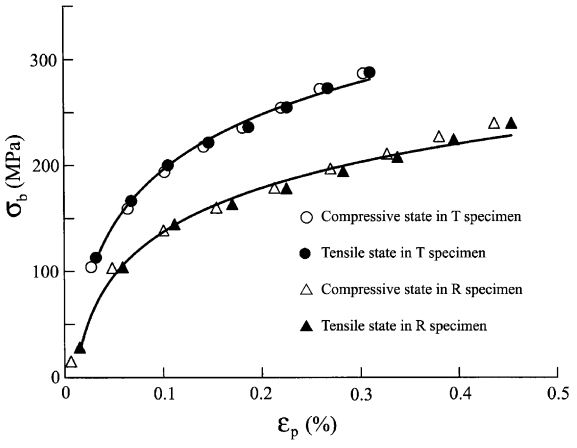

Fig. 6. Phenomenological back stress derived from the shapes of hysteresis loop.

Table 3
Parameters from the equation $\sigma_b = K^b \ln \varepsilon_p + C_b$

Sample	K^b (MPa)	C_b (MPa)	R^2
R	59.985	551.31	0.9912
T	75.244	715.44	0.9949

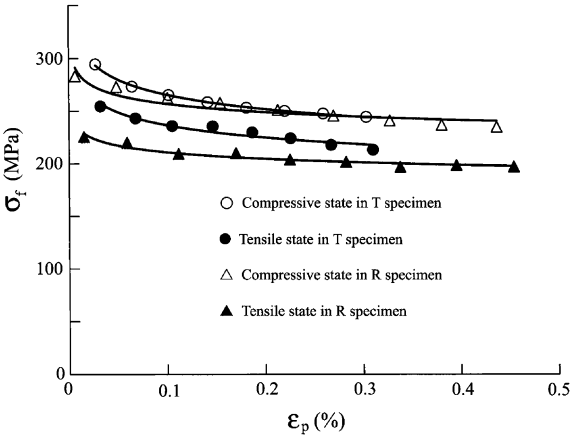

Fig. 7. Phenomenological friction stress derived from the shapes of hysteresis loop.

and the magnitude of friction stress in compression is always higher than that in tension. While, the stress difference between tension and compression is higher in R specimen. Moreover, the magnitude of σ_f^c for R specimen is always lower than T specimen whereas the magnitude of σ_f^t for both samples is close to each other at higher ε_p.

4. Discussion

4.1. Deformation mechanisms in zirconium and zirconium alloys

As a basis for discussion, the deformation systems in the α-structure of zirconium and its alloys shall be recognized.

Tenckhoff [18] reviewed the deformation systems for α-structure of zirconium and its alloys, which follow two main deformation mechanisms, slip and twinning. Under tensile or compressive stress perpendicular to *c* axis,

prismatic slip $\{10\bar{1}0\}\langle 1\bar{2}10\rangle$ is activated primarily at least at room temperature and above, up to 500 °C. At higher strain and/or elevated temperatures pyramidal slip $\{1\bar{1}01\}\langle\bar{2}113\rangle$ appears under restraint conditions, and basal slip $\{0001\}\langle 1\bar{2}10\rangle$ would exist under certain circumstances. Furthermore, under tensile stresses in the c direction, primarily $\{10\bar{1}2\}\langle\bar{1}011\rangle$ twinning, and sometimes $\{11\bar{2}1\}\langle\bar{1}\bar{1}26\rangle$ twinning, are activated, while primarily $\{11\bar{2}2\}\langle\bar{1}\bar{1}23\rangle$ and $\{10\bar{1}1\}\langle\bar{1}012\rangle$ twinning would be observed when compression is applied in the c direction.

Moreover, Crépin et al. [19] determined the critical resolved shear stress at room temperature for prismatic slip, $\{10\bar{1}2\}\langle\bar{1}011\rangle$ twinning system and $\{11\bar{2}1\}\langle\bar{1}\bar{1}26\rangle$ twinning system and indicated that these values are in the same order of magnitude. These means that the activation of preferential deformation mechanisms depends mainly on the crystallographic orientation of the grains with respect to the loading direction.

Recent findings of Crépin et al. [10] indicated that twinning mechanisms are rather complicated. Both $\{10\bar{1}2\}\langle\bar{1}011\rangle$ and $\{11\bar{2}1\}\langle\bar{1}\bar{1}26\rangle$ twins appear in tension and compression during their in-situ fatigue tests for a β treated zirconium. Twins appear under tension, tend to disappear under compression, reappear during the next tension, vice versa. Thus, twinning is a deformation mechanism admitting partial reversibility. Meanwhile, they [10] reviewed that the activation of twinning is related to the grain size. For a α treated zirconium with a grain size of 15 μm, $\{10\bar{1}2\}\langle\bar{1}011\rangle$ twins will appear whereas $\{11\bar{2}1\}\langle\bar{1}\bar{1}26\rangle$ twins are hard to be detected. While, for a β treated zirconium with a grain size of 500 μm, both $\{10\bar{1}2\}\langle\bar{1}011\rangle$ and $\{11\bar{2}1\}\langle\bar{1}\bar{1}26\rangle$ twin types can be found.

For the present material with a grain size around 8 μm, it could be deduced that both prismatic slip and $\{10\bar{1}2\}\langle\bar{1}011\rangle$ twinning are activated whereas $\{11\bar{2}1\}\langle\bar{1}\bar{1}26\rangle$ twins are hard to be observed.

ψ is defined as the angle between the c axis and the loading direction. For prismatic slip in zirconium and its alloy, Schmid factor will increase with ψ increasing from 0° to 90° and have the maximum value at 90° [18,19]. Thus, prismatic slip will remain the softest slip system and most of deformation will be accommodated through prismatic a slip under the present testing condition. However, there exists a significant difference for both samples because only prismatic slip $\{10\bar{1}0\}\langle 1\bar{2}10\rangle$ would be activated for R specimen whereas $\{10\bar{1}2\}\langle\bar{1}011\rangle$ twinning, as well as prismatic slip $\{10\bar{1}0\}\langle 1\bar{2}10\rangle$, could appear in T specimen.

After finishing the cyclic test, optical microscopy showed that less than 2% of the grains contained twins in T specimen and no twin were observed in R specimen. This means that twinning contributes very little to the plastic deformation under present testing condition.

4.2. Intergranular thermal stress

In the light of the view of Crépin et al. [10], the magnitude difference in phenomenological friction stress between tension and compression (Fig. 7) should be attributed to the irreversible twinning mechanisms. Nevertheless, this assumption is in conflict with the fact that no twin were observed in R specimen that has higher difference of friction stress whereas twins appeared in T specimen that has lower difference of friction stress.

The possible mechanism involved should consider the presence of intergranular thermal stress in the present sheet.

MacEWEN and the team [20] used the neutron diffraction to determine intergranular stresses in annealed and deformed Zircaloy-2 and suggested that cooling from the annealing temperature (650 °C) to room temperature should produce intergranular thermal stress such that the basal direction is in tension and the prismatic directions are in compression because of the highly anisotropic thermal expansion of α-Zr. More recently, Pang et al. [21] determined the tensors describing the intergranular thermal stress state of the grains in Zircaloy-2 with rod texture. Turner et al. [22] used an elastoplastic self-consistent model to calculate intergranular thermal stress in Zircaloy-2 and correlated the stress differential in the tensile and compressive yield stress with the intergranular thermal stress. Findings of Ortiz et al. [23] indicated that intergranular thermal stress in a textured zirconium could affect macrostresses measurements by approximately 60 MPa.

Accordingly, it is believed that intergranular thermal stress arises from thermal anisotropy in the present sheet. A complete thermal contraction along the c axis is prevented by the neighboring grains, which induces compressive stresses along the prismatic directions and tensile stresses along the basal direction, and lower annealing temperature corresponds to lower intergranular thermal stress provided that the cooling rate is identical and thermal stresses among grains are free at annealing temperature. Under present testing conditions, one can define an intergranular thermal stress σ_{th} such that σ_{th} will act on dislocations and its magnitude and sign remain unchanged at any point in a given hysteresis loop. Essentially, σ_{th} is an average principle intergranular stress. Then, it could be accepted from the Cottrell scheme that σ_{th} is equal in sign to σ_b^t in the tension-loading direction, and opposite to σ_b^c in the compression-loading direction. Thus, Eqs. (1) and (2) can be rewritten as the following relations:

$$\sigma_y^t = \sigma_{if}^t - (\sigma_{ib}^t + \sigma_{th}), \tag{9}$$

$$\sigma_s^t = \sigma_{if}^t + (\sigma_{ib}^t - \sigma_{th}), \tag{10}$$

then,

$$\sigma_{if}^{t} = (\sigma_{s}^{t} + \sigma_{y}^{t})/2 + \sigma_{th} = \sigma_{f}^{t} + \sigma_{th}, \tag{11}$$

$$\sigma_{ib}^{t} = (\sigma_{s}^{t} - \sigma_{y}^{t})/2 = \sigma_{b}^{t}, \tag{12}$$

where σ_{if}^{t} and σ_{ib}^{t} are referred to intrinsic friction stress and intrinsic back stress in the tension-loading direction, respectively.

Note that the sign of σ_{th} is opposite to that of σ_{b}^{c} in the compression-loading direction of the cycle, then

$$\sigma_{y}^{c} = \sigma_{if}^{c} - (\sigma_{ib}^{c} - \sigma_{th}), \tag{13}$$

$$\sigma_{s}^{c} = \sigma_{if}^{c} + (\sigma_{ib}^{c} + \sigma_{th}), \tag{14}$$

therefore,

$$\sigma_{if}^{c} = (\sigma_{s}^{c} + \sigma_{y}^{c})/2 - \sigma_{th} = \sigma_{f}^{c} - \sigma_{th}, \tag{15}$$

$$\sigma_{ib}^{c} = (\sigma_{s}^{c} - \sigma_{y}^{c})/2 = \sigma_{b}^{c}. \tag{16}$$

Similarly, σ_{if}^{c} and σ_{ib}^{c} are referred to intrinsic friction stress and intrinsic back stress in the compression-loading direction, respectively.

Combining Eq. (11) with Eq. (15), one can have

$$\sigma_{th} = (\sigma_{if}^{t} - \sigma_{if}^{c})/2 - (\sigma_{f}^{t} - \sigma_{f}^{c})/2, \tag{17}$$

Friction stress is taken equivalent to the critical stress for dislocation displacement and independent of straining direction for a given single crystal [8], so it might be assumed that the intrinsic friction stress between the tension-loading and compression-loading directions is identical, i.e. $\sigma_{if}^{t} = \sigma_{if}^{c}$. Hence, Eq. (17) can be converted into

$$\sigma_{th} = (\sigma_{f}^{c} - \sigma_{f}^{t})/2. \tag{18}$$

Thus, σ_{th} can be obtained, which is shown in Fig. 8. Note that the sign of the intergranular thermal stress σ_{th} is negative. σ_{th} in R specimen is always higher than that in T specimen at the same ε_{p}, being less than 30 MPa in R specimen and less than 20 MPa in T specimen, which are well in accordance with the findings of Pang et al. [21].

Pang et al. [21] used neutron diffraction to measure the intergranular thermal stress in textured Zircaloy-2 rod, which was annealed at 650 °C for about 4 h and subsequently followed by cooling to room temperature. They indicated all the values of tensors describing the residual thermal stress state of the grains, namely, $\sigma_{[1\,0\,\bar{1}\,0]} = -41$ MPa, $\sigma_{[\bar{1}\,2\,\bar{1}\,0]} = -3$ MPa, and $\sigma_{[0\,0\,0\,2]} = +67$ MPa. Lower annealing temperature would correspond to lower intergranular thermal stress, so the values of these tensors in the present sheet, annealed at 580 °C for 2 h and subsequently followed by cooling to room temperature, would be lower correspondingly. The prismatic directions are more concentrated in the rolling direction as compared to those in the transverse direction while basal direction is almost parallel to the normal of the sheet (Fig. 2), so the magnitude of σ_{th} would be higher in the rolling direction though the intergranular stresses balance when integrated over all grain orientations.

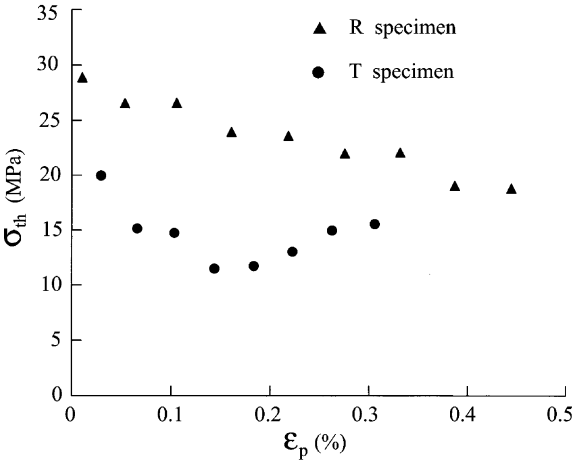

Fig. 8. Intergranular thermal stress versus plastic strain amplitude.

With increasing ε_{p}, σ_{th} in R specimen decreases, whereas σ_{th} in T specimen decreases then increases. These imply that intergranular thermal stress will evolve during the subsequent plastic deformation. Gloaguen et al. [24] reported some findings on the evolution of intergranular stress in rolled Zr702α.

As indicated in Fig. 6, magnitude of σ_{b} is little dependent of the loading direction. Therefore, one can have the following equation:

$$\sigma_{s}^{c} - \sigma_{s}^{t} = \sigma_{f}^{c} - \sigma_{f}^{t}. \tag{19}$$

Combining Eqs. (11) and (15) with Eq. (19), one can have

$$\sigma_{s}^{c} - \sigma_{s}^{t} = (\sigma_{if}^{c} - \sigma_{if}^{t}) + 2\sigma_{th}, \tag{20}$$

σ_{if}^{c} and σ_{if}^{t} should be equal to each other as mentioned above, so

$$\sigma_{s}^{c} - \sigma_{s}^{t} = 2\sigma_{th}. \tag{21}$$

It is evident from Eq. (21) that the asymmetry of stress response is largely due to the presence of intergranular thermal stress.

4.3. Back stress

Back stress is a long-range internal stress, interpreted as the existence of long-range interactions generally explained by a 'composite model', in which the crystal is considered as a composite consisting of hard dislocation

walls of high local dislocation density which are separated by soft regions of low local dislocation density [25].

Furthermore, Feaugas [26] separated the back stress into two components, namely the intragranular back stress component and the intergranular back stress component. The intragranular back stress arises from the heterogeneous dislocation distribution inside the grains and could be explained by the composite model. The intergranular back stress, however, stems: 'firstly, from grain boundary region where dislocations are generated in the neighbouring grain, emission from ledges in grain boundaries and dislocations passing across grain boundary, and secondly, from plastic strain incompatibilities between grains in relation to crystallographic orientations' [27].

A particular grain in a polycrystalline aggregate begins to deform plastically only when five independent slip systems are activated [28]. Hence, the stress state required to activate slip/twinning will vary from grain to grain, depending on the crystallographic orientations of the grains with respect to the loading axis, and some grains will accumulate plastic strains whereas others deform elastically with fewer than five activated slip systems. As for zirconium and its alloy, there are very few deformation systems and the yield surface is highly anisotropic, permitting reasonably to assume that the back stress at the lower plastic strain amplitude arises mainly from the interactions among grains, i.e. the intergranular back stress. The similar assumptions had been suggested by MacEwen et al. [29] and Hutchinson [30], and modeled schematically by Christodoulou [31]. More recently, Pang et al. described in detail the origin of the intergranular stresses in Zircaloy-2 [21]. Therefore, it could be deduced that more remarkable difference in crystallographic orientations of grains and/or much dislocation pile-ups against the grain boundaries result in higher intergranular back stress in zirconium and its alloys. Otherwise, once the dislocation walls and cell structures appear at higher plastic strain amplitude, the composite effect might be taken as one of the origins of back stress.

Therefore, the experimental fact that the back stresses for either specimen is the same for tension-loading and compression-loading implies that the strain incompatibilities among grains is little dependent of the loading direction during the cyclic deformation test.

With the aid of the relationship [18,19] between the Schmid factor and ψ, it is obviously that the sheet has a significant difference in the distribution of the Schmid factors between the rolling and transverse directions. The average value of the Schmid factors in the rolling direction is higher and the Schmid factors distribution is more concentrated than that in the transverse direction. These allow to assume that more grains of the aggregate will be oriented favorably for slip and subjected to plastic deformation under the loading in the rolling direction as compared to those in the transverse direction at the same plastic strain amplitude. In another word, less grains of the aggregate, under the loading in the transverse direction, are responsible for the plastic deformation, and therefore these grains experience much plastic deformation, thus leading to higher plastic strain incompatibilities between grains and much dislocations pile-up against the grain boundaries. So, T specimen exhibits higher back stress than R specimen.

The increase of back stress with the plastic strain amplitude could be attributed to the twofold. One is from the dislocation pile-up against the grain boundary. Indeed the grain boundaries act as strong barriers to slip and dislocation pile-ups against a grain boundary impose a stress concentration and the number of dislocations in the pile-up will increase with the plastic strain. Accordingly, the stress concentration increases with increasing the plastic strain, leading to higher intergranular internal stress. The other is from the plastic strain incompatibilities between grains. The plastic strain incompatibilities will become more remarkable with plastic strain.

However, the question that the back stress increases logarithmically with plastic strain amplitude (Eq. (8)) as yet remain unanswered.

4.4. Friction stress

As can be seen from Eq. (18), the difference of phenomenological friction stress between tension (σ_f^t) and compression (σ_f^c) is mainly from the intergranular thermal stress. As narrated above, the texture effect results in the difference in the average principle intergranular stress σ_{th} between rolling and transverse directions, namely, magnitude of σ_{th} in the rolling direction is higher. So, the difference of phenomenological friction stress is higher in R specimen.

Combining Eq. (11) with Eq. (15), one can have the following relation:

$$\sigma_{if}^t + \sigma_{if}^c = \sigma_f^t + \sigma_f^c, \tag{22}$$

σ_{if}^t should be equal to σ_{if}^c as narrated above, thus the intrinsic friction stress σ_{if} is obtained, i.e.

$$\sigma_{if} = (\sigma_f^t + \sigma_f^c)/2. \tag{23}$$

So, one can have the intrinsic friction stress versus the plastic strain amplitude, as shown in Fig. 9. σ_{if} is higher in T specimen than that in R specimen and σ_{if} for both samples decreases slightly with increasing ε_p, which could be tentatively explained as the following.

From the view of Feaugas et al. [26,27], the friction stress in the polycrystalline aggregate corresponds to the radius of the yield surface in stress space. Hence, friction stress should be related considerably to the grain

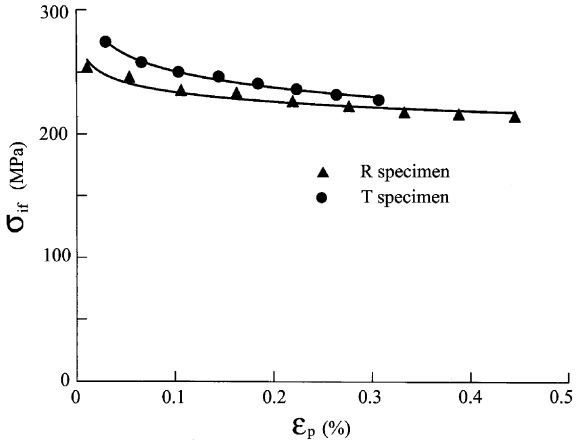

Fig. 9. Intrinsic friction stress versus plastic strain amplitude.

orientation. In the present sheet, the Schmid factors is higher in R specimen, resulting in lower friction stress. However, the reason that the friction stress decreases slightly with increasing the plastic strain amplitude could be attributed to the grain-rotation, which was demonstrated in Refs. [2,9].

The saturated stress comprises phenomenological back and friction stresses. As indicated above, phenomenological back stress increases logarithmically (Fig. 6) whereas phenomenological friction stress decreases slightly (Fig. 7) with increasing ε_p, which mean that the increase of saturated stress with ε_p (Fig. 5) stems from the strain incompatibilities between grains. In another word, the materials hardening behavior results from the strain incompatibilities between grains.

5. Conclusions

The preceding discussion has shown that the cyclic deformation behavior observed in this study can be correlated to intergranular thermal stress and basic deformation mechanisms operating in zirconium and its alloys.

In both the rolling and transverse directions the material exhibits an asymmetry of stress response under cyclic deformation. The asymmetry of stress response in rolling direction is more pronounced than in transverse direction. The cyclic stress–strain curves could be expressed as the power law relation $\sigma_s = K^s \varepsilon_p^{n^s}$ for either tension or compression directions.

In both directions, the magnitude of phenomenological friction stress in compression is always higher, and the difference between σ_f^c and σ_f^t is more pronounced in rolling direction than that in transverse direction. While the magnitude of phenomenological back stress is independent of the loading direction, increases much more rapidly in transverse direction than in rolling direction with the plastic strain amplitude, and the trend in both directions could be expressed as the logarithmic relation $\sigma_b = K^b \ln \varepsilon_p + C_b$.

The difference between σ_f^c and σ_f^t, which contributes to the asymmetry of stress response, could be largely attributed to the presence of intergranular thermal stress in the present sheet.

However, back stress is primarily a direct consequence of the plastic strain incompatibilities between grains.

The different performance between rolling and transverse directions results from the texture effect.

Acknowledgements

Financial support from the Chinese national key laboratory Foundation and NPIC (Nuclear Power Institute of China) youth Foundation is gratefully appreciated.

References

[1] L. Caillot, B. Linet, C. Lemaignan, in: Transactions of the Twelfth International Conference on Structural Mechanics In reactor Technology, Amsterdam, 1993, C04/2, p. 69.
[2] D.H. Lee, S.I. Kwun, Scr. Metall. Mater. 31 (1994) 1475.
[3] Xiao Lin, Gu Haicheng, Fatigue 16 (1994) 417.
[4] G. Brun, J. Pelchat, J.C. Floze, M. Galimberti, in: Zirconium in the Nuclear Industry, Seventh International Symposium, ASTM STP 939, American Society for Testing and Materials, Philadelphia, 1987, p. 597.
[5] W.J. O'Donnell, B.F. Langer, Nucl. Sci. Eng. 20 (1964) 1.
[6] Xiao Lin, Gu Haicheng, J. Nucl. Mater. 265 (1999) 213.
[7] A.H. Cottrell, Dislocations and Plastic Flow in Crystals, Oxford University Press, London, 1953, p. 111, 132.
[8] D. Kuhlmann-Wilsdorf, C. Laird, Mater. Sci. Eng. 37 (1979) 111.
[9] H.I. Choi, D.H. Lee, S.I. Kwun, Scr. Mater. 38 (1998) 565.
[10] J. Crépin, T. Bretheau, D. Caldemaison, F. Ferrer, Acta Mater. 48 (2000) 505.
[11] O.B. Pedersen, J.V. Carstensen, Mater. Sci. Eng. A 285 (2000) 253.
[12] E. Tenckhoff, in: Zirconium in the Nuclear Industry, Fifth Conference, ASTM STP 754, American Society for Testing and Materials, 1982, p. 5.
[13] J.J. Kearns, Thermal expansion and preferred orientation in Zircaloy, WAPD-TM-472, Westinghouse Electric Corp., Pittsburgh, PA, November 1965.
[14] K.L. Murty, in: Zirconium in the Nuclear Industry, Eighth International Symposium, ASTM STP 1023, American Society for Testing and Materials, Philadelphia, 1989, p. 570.
[15] E. Tenckhoff, P.L. Rittenhouse, J. Nucl. Mater. 35 (1970) 14.
[16] S.B. Wisner, M.B. Reynolds, R.B. Adamson, in: Zirconium in the Nuclear Industry, Tenth International Symposium, ASTM STP 1245, American Society for Testing and Materials, Philadelphia, 1994, p. 499.

[17] ASTM standard E606. Standard Recommended Practice for Constant-amplitude Low-cycle Fatigue Testing.
[18] E. Tenckhoff, Deformation mechanisms, texture, and anisotropy in zirconium and Zircaloy, ASTM STP 966, 1988.
[19] J. Crépin, T. Bretheau, D. Caldemaison, Acta Metall. Mater. 43 (1995) 3709.
[20] S.R. MacEWEN, J. Faber Jr, A.P.L. Turner, Acta Metall. 31 (1983) 657.
[21] J.W.L. Pang, T.M. Holden, P.A. Turner, T.E. Mason, Acta Mater. 47 (1999) 373.
[22] P.A. Turner, N. Christodoulou, C.N. Tome, Int. J. Plast. 11 (1995) 251.
[23] M. Ortiz, A.A. Pochettino, J. Nucl. Mater. 229 (1996) 65.
[24] D. Gloaguen, M. Francois, R. Guillen, J. Royer, Acta Mater. 50 (2002) 871.
[25] H. Mughrabi, Acta Metall. 31 (1983) 1367.
[26] X. Feaugas, Acta Mater. 47 (1999) 3617.
[27] X. Feaugas, C. Gaudin, Mater. Sci. Eng. A 309&310 (2001) 382.
[28] R.W.H. Honeycombe, Plastic Deformation of Metals, Cambridge University Press, Cambridge, 1964.
[29] S.R. MacEWEN, C.E. Ells, O.T. Woo, J. Nucl. Mater. 101 (1981) 336.
[30] J.W. Hutchinson, J. Mech. Phys. Solids 12 (1964) 11.
[31] N. Christodoulou, Acta Metall. 37 (1989) 529.